# The role of feldspar and pyroxene minerals in the ice nucleating ability of three volcanic ashes

Leif G. Jahn[1], William D. Fahy[1], Daniel B. Williams[2], Ryan C. Sullivan[1,*]

[1]Center for Atmospheric Particle Studies, Carnegie Mellon University, Pittsburgh, Pennsylvania, USA

[2]Department of Geology and Environmental Science, University of Pittsburgh, Pittsburgh, Pennsylvania, USA

*Correspondence to:* Ryan C. Sullivan (rsullivan@cmu.edu)

## Abstract

The mineralogical and immersion-mode freezing properties of volcanic ashes from three volcanoes – Volcán de Fuego and Santiaguito in Guatemala, and Soufrière Hills Volcano, in Montserrat – were examined. All ashes (sieved to <37 μm) contained effective ice nuclei, typically freezing over the temperature range of –12 to –25 °C and possessing ice active site densities ($n_s$) spanning ~$10^1$-$10^5$ $cm^{-2}$ over this temperature range. The high freezing activity of the ashes was determined to likely originate from pyroxene minerals, and the ice nucleation properties of pyroxene minerals are also reported here for the first time for comparison. Ca- and Na-rich plagioclase feldspars also contributed to the observed freezing properties. Volcanic glass was present in all of the samples and is theorized to be a much weaker ice nucleant, effectively diluting the freezing ability of the crystalline mineral phases. Smaller particle size fractions of the Volcán de Fuego ash were observed to contain more active ice nucleating particles, attributed to an increase in the amount of pyroxene minerals with decreasing particle size fractions. The particle re-suspension and size segregated collection process was also observed to increase the ice nucleating ability of all size fractions, likely due to mechanical ablation removing passivated surfaces and exposing fresher and more ice-active mineral surfaces.

KEYWORDS: heterogeneous ice nucleation, volcanic ash, mineralogy, immersion freezing, single-particle analysis, aerosol-cloud interactions, atmospheric chemistry

## 1 Introduction

Volcanic ash represents a major periodic source of mineral material emitted to the atmosphere, consisting of a mixture of crystalline components and amorphous glassy material.[1,2] Large volumes of ash are ejected into the atmosphere during intense explosive eruptions, but some volcanoes also eject smaller quantities of ash at more frequent intervals.[3,4] After injection into the atmosphere, ash settles out of the atmosphere during transport to downwind regions. Ashes can serve as ice nucleating particles both near the point of origin[5] and in downwind regions.[6] The freezing ability of ash particles is relevant to a variety of processes, including the dynamics of ash aggregation and settling,[7–9] the evolution of volcanic clouds,[1,7,10] the occurrence of volcanic lightning,[11] and, ultimately, the dynamics of air masses downwind of the ash plume.

Ash particles can persist in the atmosphere hundreds to thousands of kilometers from the volcano[12] and exert a clear influence on ambient ice nucleating particle (INP) concentrations.[6,13]

To understand and model these ice nucleation (IN) processes and their resulting effects, some knowledge is required of the properties of volcanic ash particles and the supercooled temperatures over which they can initiate freezing. Freezing on mineral particles can be influenced by a number of surface attributes, including the presence and arrangement of hydroxyl groups,[14–16] the exposed crystal lattice,[17,18] geometric features such as pores and cracks,[15,19,20] and surface charge,[21,22] although the relative importance of and interplay between these properties remains an ongoing area of research.[15,23,24] A variety of mineral phases can be present in volcanic ashes, including amphiboles, olivines, pyroxenes, feldspars, micas, and silica polymorphs, in addition to amorphous volcanic glass.[1,25,26] Amphiboles, olivines, and pyroxenes tend to weather relatively quickly[27] and are generally not observed in atmospheric mineral dust particles. Natural chemical weathering of mineral phases occurs when minerals are exposed to reactants such as water, acid, or dissolved ions which degrade the original mineral and lead to the formation of more stable phases. Clay minerals tend to be the most common end products of natural weathering.[28–31]

Previous research has shown that feldspar phases can be one of the more common mineral components in atmospheric volcanic ash particles.[1,32–34] Feldspars are tectosilicate minerals and are broadly divided into two categories: plagioclase ($NaAlSi_3O_8$-$CaAl_2Si_2O_8$) and alkali ($NaAlSi_3O_8$-$KAlSi_3O_8$). Each exists as a solid solution with an elemental composition somewhere between the two pure endmember species. Feldspars are common components of mineral dust[30,31,35] and are postulated to be a significant contributor to atmospheric INP concentrations.[19,36–40] The freezing abilities of feldspars have been thoroughly surveyed and show the general trend that alkali feldspars exhibit more active freezing ability than plagioclase feldspars.[19,37] A recent study suggested that perthitic microtextures – created by phase separation between Na- and K-rich regions that commonly occur in alkali feldspars – are the strongest indicator of the ability to freeze over the temperature range of around -3 to -15 °C with active site densities ($n_s$) < $10^3$ $cm^{-2}$ that is observed in some highly ice-active alkali feldspars.[41] These features provide a site for chemical attack and dissolution, which gives rise to a variety of topographical features at the grain boundary. These features then serve as ice-active sites, either due to the geometry of the features themselves,[42] the functional group arrangements or lattice planes found at the sites and features,[20] or possibly a combination of the two.[15,41] Perthitic microtextures originate from the exsolution (phase separation) of a mineral species into regions with distinct composition, which depends on the phase formation temperature and cooling rate. In alkali feldspars, perthitic microtextures are most commonly visible as sodium-rich albite lamellae within a potassium-rich orthoclase phase.[41] However, exsolution and the presence of perthitic microtextures are not unique to alkali feldspars. They can also occur in a variety of other minerals, including those commonly observed in volcanic ashes such as olivines, amphiboles, and pyroxenes.[43,44]

Significant quantities of the pyroxene phase enstatite have been observed in ash from the Soufrière Hills volcano.[32,33] Pyroxenes are inosilicate minerals with the general formula $XYSi_2O_6$, where X and Y are most commonly magnesium, iron, or calcium. A solid solution exists among these phases, similar to feldspars, with the ideal composition of $XYSi_2O_6$. The X site is ideally occupied by either Mg or Fe, while the Y site is ideally occupied by Mg, Fe, or Ca. Enstatite is the pure magnesium pyroxene endmember and has the formula $Mg_2Si_2O_6$. Pyroxene minerals can be common in volcanic ashes but are rarely found in desert dust or atmospheric mineral dust. Volcanos may thus represent a unique source of pyroxene minerals to the atmosphere, and the ice nucleation properties of these mineral phases have not been examined in detail to our knowledge. Recent work with volcanic tephra (volcanic material of broad origin) suggests that some pyroxene phases can initiate freezing at temperatures near -10 °C.[45]

Historically, a range of ice-nucleation behaviors have been observed for volcanic ashes from different volcanoes.[46] These authors also observed some ice-active behavior from pyroxene mineral samples. The freezing activity of volcanic ashes has been explored in greater detail in recent studies. Durant et al. (2008) examined the freezing of a series of supermicron ash particles from different types of volcanoes and came to the conclusion that volcanic ashes will generally nucleate ice over the range –13 to –23 °C in the immersion mode. A number of publications have examined the ice nucleation properties of ash from the 2010 Eyjafjallajökull eruptions.[34,47–49] Zolles et al. (2015) observed freezing activity comparable to that of Na-rich plagioclase feldspars, which comprised about 70% of the ash composition.[47] Steinke et al. (2011) and Hoyle et al. (2011) examined ash in the deposition and immersion regimes and observed freezing behavior similar to that of natural mineral dusts.[48,49] Kulkarni et al. (2015) compared this ash to Arizona test dust (ATD: a processed mixture of quartz, clay, feldspar, and calcite) and concluded that amorphous glass content in the ash imparted weaker freezing ability compared to ATD despite similar mineral and elemental content.[34] A similar conclusion was reached by researchers studying volcanic glass from the Santorini volcano, Italy who determined that glass can serve as an ice nucleant but has weaker activity than feldspar minerals, based on an observed lower critical freezing temperatures.[50] Maters et al. (2019) observed weaker freezing in glass synthesized from volcanic tephra than from the parent tephra.[45] Harrison et al. (2016) also directly compared the IN ability of a glassy synthetic anorthite (plagioclase feldspar) and its crystalline counterpart and observed the glassy material to have weaker freezing ability.[37]

Most recently Mangan et al. (2017) examined ash from the Soufrière Hills volcano and observed relatively strong freezing ability, comparable to that of highly ice-active alkali feldspar minerals, without observing any alkali feldspars in the ash composition.[33] The authors also compiled the results from a number of freezing studies on volcanic ash, showing that ashes from different volcanoes can be ice active in a wide range of temperature regimes. Notably, the results differ greatly from previous freezing experiments with ash from the Soufrière Hills volcano,[32] where in the immersion mode ash froze near the background freezing limit of the measurements. In this work we analyze three volcanic ash samples from Guatemala and Montserrat in the Caribbean to determine their ice nucleating ability, crystalline phase composition, and

amorphous glass content with the goal of elucidating the origin of any IN activity in the ash samples and investigating possible reasons for observed differences in the IN abilities of ash samples previously reported from the same volcano.

## 2 Materials and methods

Each ash sample was collected from the respective location following an eruption or ashfall event in the stated year: Belham Valley near the Soufrière Hills volcano (hereinafter SHV), Montserrat in 2010; the El Brujo dome of Santiaguito, Guatemala in 2011; and Volcán de Fuego (hereinafter Fuego), Guatemala in 2015. These samples are held at the Image Visualization and Infrared Spectroscopy (IVIS) Laboratory at the University of Pittsburgh as part of the ASTER Volcanic Ash Library.[51] Prior to analysis, all ash samples were sieved through 37 μm mesh (Fisher Scientific U.S. Standard Sieve Series, mesh no. 400). The naturally occurring <37 μm fraction of each ash was used for all analyses to restrict the results to particle sizes that could have appreciable atmospheric lifetimes. Additionally, some of the <37 μm Fuego ash was resuspended via dry-dispersion using a home-built dust generator[52] and passed through a series of cyclone impactors and filters to provide three distinct particle aerodynamic size fractions: 10-37 μm, 2.5-10 μm, and <2.5 μm. There were insufficient amounts of the Santiaguito and SHV samples to repeat this procedure with these ashes. The operation of this apparatus is described in the Supplemental Information and a schematic can be seen in Figure S1. Immersion-mode ice nucleation (IN) experiments were done using the previously described Carnegie Mellon University cold stage apparatus (CMU-CS).[53–55] Briefly, ash suspensions of the desired weight percentage were prepared in HPLC-grade water (Sigma Aldrich HPLC Plus #34877) that was filtered (Anotop 25 Plus 0.02 μm pore size, Whatman #6809-4102). Then, 0.10 μL droplets were pipetted onto a silianized hydrophobic coverslip (Hampton Research, HR3-231) immersed in hydrophobic squalene oil (TCI chemicals, #H0097) in an aluminum dish. A thermoelectric cooler and thermoelectric air chiller heat sink were used to control and ramp the temperature of the droplet array at 1 °C/min with an uncertainty of ±0.5 °C. Freezing experiments were done immediately after suspensions were made, and suspensions were agitated during pipetting to prevent settling. Two to three arrays of 40-60 droplets each were performed for each ash sample. We display the freezing results of each sample as an additive combination of each separate array, rather than an average of the arrays. The ash samples analyzed here are sufficiently heterogeneous that we are unsure whether each individual array will fully capture the possible freezing behaviors of each ash component. For this reason, we believe the combination approach better represents the full freezing ability of each ash. Combining as opposed to averaging replicate droplet arrays increases droplet statistics and typically does not significantly alter the retrieved properties such as median freezing temperature or the $n_s$ spectrum.[54]

Brunauer-Emmett-Teller (BET) specific surface area (SSA) measurements were made via nitrogen gas adsorption with a Micromeritics Gemini VII 2390 porosimeter. X-ray diffraction (XRD) measurements were performed on a PANalytical X'Pert Pro MPD diffractometer. A copper X-ray source was used, and all scans were done over the °2$\theta$ range of 10°-70° with a step size of

0.013°. Relative mineral phase amounts were determined via Rietveld refinement using the spectra available in the crystallography open database (COD, http://www.crystallography.net/cod/) and the International Centre for Diffraction Data database (ICDD, http://www.icdd.com/). Feldspar minerals of similar composition (e.g. anorthite and bytownite) were grouped together owing to similarities in their spectra and difficulty distinguishing between the two phases. Raw XRD results are provided in the Supplementary Information in Figure S3.

A relatively pure sample of the pyroxene mineral augite was purchased (Ward's Science, #470025-746) to use as a standard material for determining the ice nucleating ability of a pyroxene mineral phase. Augite occupies a broad space within the pyroxene solid solution, with composition varying from $MgCaSi_2O_6$ to $FeCaSi_2O_6$ and the Y site containing 15-45% calcium. To prepare the sample for IN analysis, it was first pulverized and then ground with a mortar and pestle before sieving to <37 μm. The sieved powder was characterized by XRD and BET analysis, the results of which are shown in Table S1. Rietveld refinement of the XRD spectrum indicates that ~93% by mass of the sample are pyroxene phases, mostly diopside ($CaMgSi_2O_6$) and augite, with small amounts of silica and feldspars. It is also worth noting that the sample likely contains some amount of amorphous material, judging by the size of the tail at low °2**θ** values in the XRD spectrum.

Scanning electron microscopy (SEM) and energy dispersive X-ray spectroscopy (EDX) measurements were performed with an FEI Quanta 600 field emission gun microscope. To prepare samples for SEM analysis, a small amount of ash was placed next to a piece of conductive carbon tape on an SEM stub. A small puff of air from a compressed air canister was used to aerosolize a small amount of ash, some of which stuck to the carbon tape. This was done in a laminar flow hood to avoid contamination. SEM was also used to verify particle size fractions produced via the dust generator apparatus and were found to be reliable; some sample images are provided in Figure S2. Computer-controlled measurements were acquired using the INCA software platform and several hundred particles (~200-400) were analyzed for each sample. An accelerating voltage of 10.0 kV and a spot size of 3 were used for all measurements. Polarized light microscopy (PLM) was performed by RJ Lee Group to determine the amount of amorphous glass in each ash sample and to inform XRD phase assignments. A summary of the results of the BET, XRD, and PLM results are shown in Table 1, and a graphical representation of the composition and amorphous content of the ashes is shown in Figure 1.

**Table 1**. Properties of each volcanic ash particle size sample analyzed.[a]

| Sample | BET SSA ($m^2$ $g^{-1}$) | %glass | Na-rich Plagioclase feldspar | Ca-rich Plagioclase feldspar | Alkali feldspar | Pyroxene | Silica polymorphs | Olivine | Amphibole | Magnetite |
|---|---|---|---|---|---|---|---|---|---|---|
| Fuego 2015 PM37 | 1.1314 | 20 | 14.7 | 70.1 | 3.7 | 8.7 | 0.5 | 2.2 | 0 | 0.2 |
| Santiaguito 2011 PM37 | 0.9687 | 75 | 56.8 | 17.6 | 1 | 9.6 | 13.6 | 0.2 | 0.8 | 0.4 |
| SHV 2010 PM37 | 0.4630 | 76 | 25 | 38.3 | 2.4 | 12.3 | 21.1 | 0 | 0.3 | 0.4 |
| Fuego 2015 PM10-37 | 2.3632 | - | 10.6 | 72.4 | 6.1 | 7.5 | 0.4 | 2.2 | 0.5 | 0.2 |
| Fuego 2015 PM2.5-10 | 4.961 | - | 31.2 | 48.7 | 5.6 | 11 | 0.3 | 1.5 | 1.1 | 0.5 |
| Fuego 2015 PM<2.5 | 9.1339 | - | 35.6 | 45.1 | 1 | 15.3 | 0.3 | 1.5 | 0.8 | 0.5 |

[a]A more detailed mineral phase breakdown and raw XRD spectra are provided in Table S2 in the Supplementary Information.

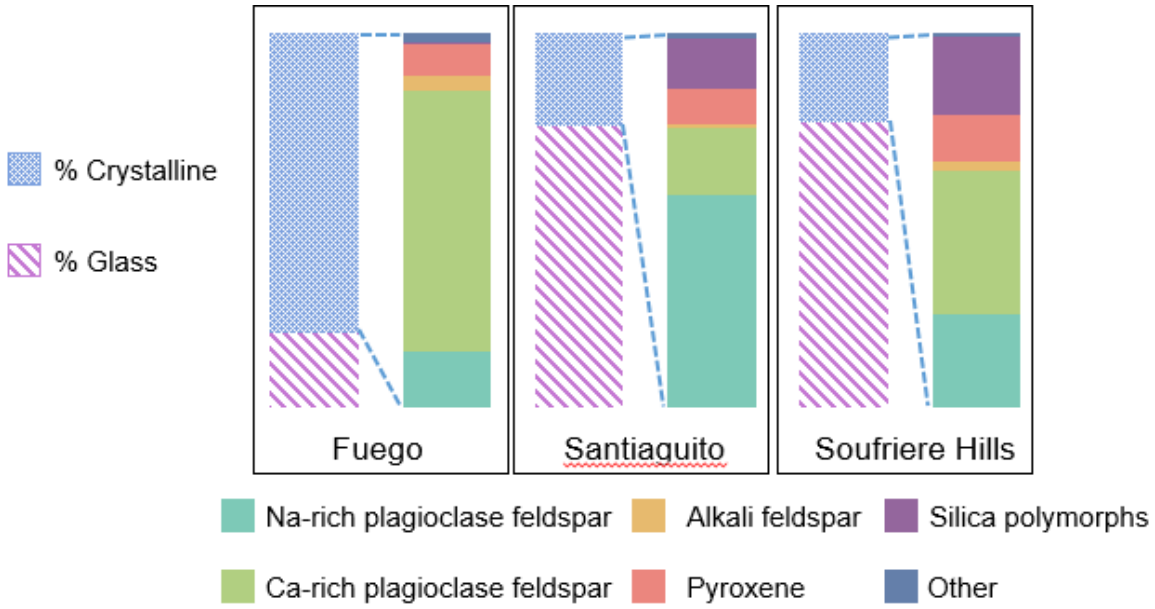


**Figure 1**. Graphical representation of the crystalline versus amorphous content and XRD crystalline phase compositional breakdown for each of the three <37 μm sieved volcanic ash samples.

## 3 Results and Discussion

### 3.1 Mineralogy and Ice Nucleation Properties of the Three Volcanic Ashes

Droplet freezing temperature spectra for 0.1 wt% and 0.01 wt% suspensions of the three sieved ashes are displayed in Figure 2, along with the average spectrum from purified water controls. All three ash samples are ice active over the range –12 to –25 °C. The INP number concentration ($c_{IN}$) cumulative temperature spectra were derived from the droplet freezing

spectra for all samples as well as for purified water controls.[56] The average $c_{IN}$ spectrum for the controls was subtracted from the $c_{IN}$ spectrum of each sample to account for interference from background freezing due to trace water impurities or droplet-substrate interactions.[54] In the pure water controls, about 20% of droplets were typically frozen by -26 °C; at colder temperatures, it becomes difficult to distinguish freezing by the sample from the system background. The surface area-to-mass ratios measured via BET analysis were used to normalize for the particle surface area in each suspension and convert $c_{IN}$ to the ice nucleation active site density ($n_S$) temperature spectrum,[1,56,57] plotted in Figure 2. Error bars are calculated from a single standard deviation of the background $c_{IN}$ spectrum.[58] Based on this, all three samples display similar freezing activity. SHV ash samples consistently finish freezing at lower temperatures than Fuego and Santiaguito ashes, indicating the SHV ash possess fewer particles that are ice active in this temperature range. Differences in glass content between the ashes (20% in Fuego versus 75% and 76% for Santiaguito and SHV, respectively) could be part of the origin of the broader freezing range of the SHV ash The SHV 0.01 wt% freezing temperature spectrum dips below the average background freezing spectrum of filtered water. We suspect the droplets freezing at and below background contain mostly glassy particles with low ice activity, which have been observed to freeze below -30 °C.[50] The active site densities for these droplets cannot be reliably determined as they cannot be distinguished from the background freezing signal. We show the complete droplet freezing temperature spectra (Fig. 2, left) but omit any data within the uncertainty of our background freezing spectrum in the $n_s$ spectra (Fig. 2, right); this only occurs for the SHV 0.01% array. The 0.01 wt% Santiaguito and SHV ash suspensions exhibit higher $n_S$ values than their 0.1 wt% counterparts, which is a phenomenon consistent with previous reports.[55,59–61] The $n_S$ metric can attain higher values when low particle concentrations are used to create droplets; at higher concentrations the diversity of ice active sites in each droplet becomes saturated, reducing the $n_s$ value retrieved.[55]

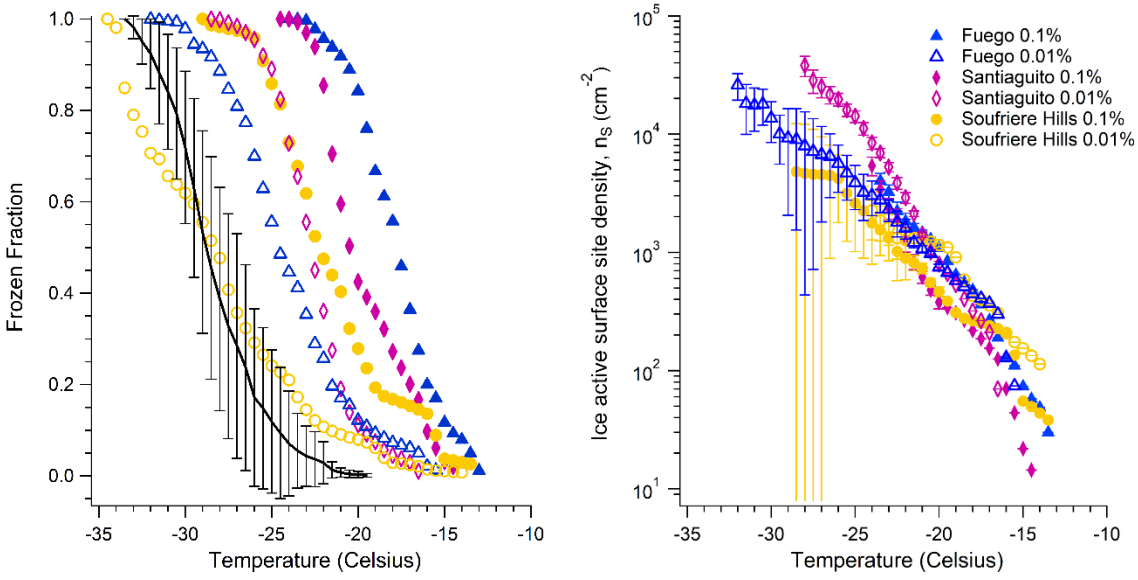

Figure 2. Droplet freezing temperature spectra showing number of droplets frozen against temperature (°C) (left); and ice active site density ($n_S$) spectra of the three volcanic ashes plotted against temperature (right). Each plot shows results for the <37 μm size fraction of each of the three volcanic ashes. Fuego is shown in blue, Santiaguito is shown in magenta, and SHV is shown in yellow. 0.1 wt% suspensions are shown in closed symbols while 0.01 wt% suspensions are shown in open symbols. The average purified water background for the CMU-CS cold stage system is shown in black, plotted with error bars showing a single standard deviation.

All of the ash samples are ice active in the temperature regime of –13 to –23 °C noted by Durant et al. (2008). However, the frozen fraction curves and $n_S$ spectra also show that many droplets froze below this temperature range. This means that those droplets did not possess an INP of sufficient activity to initiate freezing at a warmer temperature, and it follows that not all ash particles are able to initiate freezing within the aforementioned temperature range. This is especially visible in the 0.01 wt% suspensions, where the concentration of the most active INPs is diluted relative to the 0.1 wt% suspensions. The broad temperature range spanned by the frozen fraction curves and $n_S$ plots is an indication that the population of ash particles is somewhat heterogeneous, with different particles possessing characteristics that induce freezing in different temperature ranges.

These ash samples possess highly active freezing ability, freezing at temperatures as warm as the most active atmospherically relevant mineral phases. The origin of this freezing ability is not immediately clear. Comparison to previously compiled feldspar mineral $n_s$ freezing spectra[19,35,37] indicates that our samples have weaker freezing activity than the most ice-active alkali feldspars but higher activity than plagioclase feldspars. The major crystalline phase in each sample is plagioclase feldspar, which could be the source of freezing activity over the range ~ -17-25 °C[37,62] but can't explain the warmest freezing in our samples. The silica polymorphs present in the Santiaguito (tridymite) and SHV (cristobalite) ashes could be ice active over the temperature ranges of our samples, although we find no prior direct measurements of their IN abilities. A lattice match exists between hexagonal ice and β-tridymite and cubic ice and β-cristobalite, but these polymorphs are not stable at low temperatures and we do not expect them to be present in our samples.[63] The freezing ability of another silica polymorph, quartz, has been examined previously and has been observed to be highly variable, with the warmest IN activity attributed to surface roughening and milling.[47,64] However, we suspect that the silica polymorphs in the Santiaguito and SHV ashes do not contribute significantly to the IN behavior observed in this work. Unmilled quartz has been observed to be a weaker ice nucleant than plagioclase feldspars,[35,47,64] and our ash samples were not milled or ground. Additionally, the similar freezing behavior and bulk composition of all three ashes suggest that these small differences in composition do not play a role in determining the IN behavior of the Santiaguito and SHV ashes. Overall, this suggests that the warmest freezing behavior in our samples is due to one of the minor mineral components with higher IN activity than plagioclase. Alkali feldspars

in the samples could contribute to the warm freezing activity observed at temperatures near –10 °C, but the small amounts of these phases (~1-4% by XRD) make it unlikely that they are the sole source of the freezing activity. We base this conclusion on a rough scaling of the range of $n_S$ values (~ $10^1$ to $10^3$ $cm^{-2}$) previously measured for alkali feldspars over the temperature range –10 to –15 °C.[19,35,37] These literature measurements were done on pristine ground alkali feldspar samples, so we take them as a likely upper bound for what could be observed in our ambient collected particles.

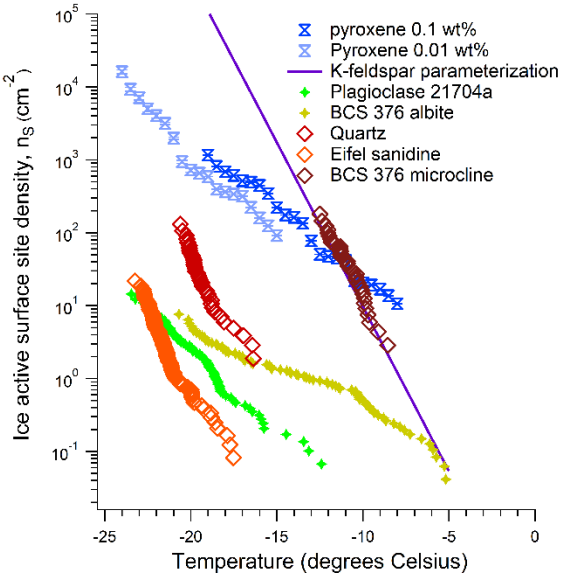


**Figure 3**. Ice active site density ($n_S$) spectrum of a pure pyroxene mineral (diopside/augite) sample (blue bow ties). Also shown are $n_S$ curves from a parameterization of K-rich feldspar,[35] a Ca-rich plagioclase feldspar (21704a) (green diamonds),[37] an Na-rich albite (BCS 376) (yellow diamonds),[37] a K-rich Eifel sanidine feldspar (orange open diamonds),[65] a K-rich microcline feldspar (burgundy open diamonds),[65] and a quartz sample (red open diamonds).[65]

The ice nucleating ability of pyroxene minerals, ~8-13% in these ashes by XRD, are relatively unknown and a pyroxene sample was thus analyzed to determine the possible contribution of these phases. The droplet freezing temperature spectra and $n_S$ plots for the diopside/augite pyroxene sample acquired are shown in Figure 3. Also shown are several $n_S$ plots for previously compiled mineral phases, including alkali[35] and plagioclase feldspar.[37] As can be seen, our pyroxene standard is very efficient at nucleating ice, freezing over the general range –10 to –20 °C. The $n_S$ spectra also occupy the same space as the spectra of our volcanic ash samples. Based on this, we attribute the highly active freezing ability of our ashes to the pyroxene phases in our samples. The causes of the strong IN ability of the pyroxene material is unknown but could be due to any of the variety of mineralogical properties mentioned in the introduction, such as crystal lattice match, surface functional group distribution, and topographical features. The pyroxene studied here is one of the few mineral phases that has been observed to nucleate

ice above –10 °C, along with some alkali feldspar phases. One possible explanation for the warmest freezing behavior in this pyroxene is that this ability has a similar origin as that of the alkali feldspars. That is, especially warm freezing activity with low active site densities results from perthitic microtextures and originates at grain boundaries between exsolved phases. Although exsolution can commonly occur in pyroxene phases,[44,66] it is certainly possible that the freezing ability of this particular pyroxene may not be representative of all pyroxene phases.

Computer-controlled scanning electron microscopy with energy dispersive x-ray spectroscopy (CCSEM/EDX) was used to probe the distribution of pyroxene phases among individual volcanic ash particles. Magnesium and iron were used as markers for the presence of pyroxenes in these particles, as these elements would be expected to exist in other phases in relatively insignificant amounts. Calcium may be present in particles either as feldspar or pyroxene, while sodium is most likely present as feldspar. Two caveats to this analysis are the unknown elemental composition of the glassy material, which could be similar to the crystalline components or closer to pure silica, and the fact that these elements may be present in some of the minor mineral phases in each sample. Particle compositions are interpreted as ternary plots of the relative amounts of (magnesium+iron)–calcium–sodium and are shown in Figure 4.[67] Particles that contained a small amount (<0.1 wt%) of magnesium, iron, calcium, and sodium were omitted from the ternary diagrams.

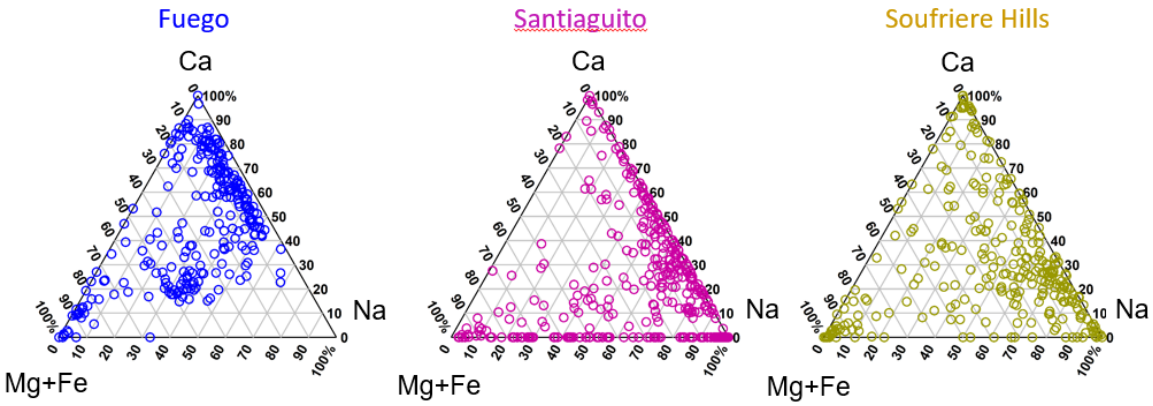


**Figure 4**. Ternary plots of the relative amounts of the elements (Mg+Fe)-Ca-Na in the three <37 μm ash samples acquired via CCSEM/EDX. Colors are as before; Fuego is shown on the left, Santiaguito is shown in the middle, and SHV is shown on the right. Each point represents the elemental ratio of (Mg+Fe)-Ca-Na for a single particle.

Overall, these ternary diagrams show agreement with the bulk compositions determined by XRD. Calcium is the major element in Fuego particles, consistent with Ca-rich plagioclase as the dominant phase; sodium is the major element in Santiaguito particles, consistent with Na-rich plagioclase as the dominant phase; and the elemental distribution in SHV particles is more balanced, consistent with the more similar amounts of calcium and sodium rich plagioclases. Particles clustered along the Ca–Na axis are indicative of pyroxene-poor particles, while particles

clustered towards the Mg+Fe corner are relatively pyroxene-rich. Particles in the middle of the diagrams may possess a mixture of mineral phases and may also contain calcium-substituted pyroxenes. An example of such a particle is shown in Figure 5. The ternary plots show that while a number of particles contain magnesium and/or iron and may contain pyroxene phases, many more particles do not. This indicates that pyroxenes – the likely origin of the highly active IN behavior in these samples – are not present in all particles. Thus, not all droplets in the freezing arrays may contain highly ice-active particles, which will broaden the temperature range over which the ashes freeze relative to the pure pyroxene sample. We conclude that the temperature ranges over which the ashes are observed to freeze are due to the multiple phases within each sample. The pyroxene phases are the most common ice-active material and initiate freezing at warmer temperatures, while droplets that do not contain pyroxene phases freeze at colder temperatures due to plagioclase feldspars.

The elemental maps shown in Figure 5 for a single ash particle from Volcán de Fuego make it clear that multiple distinct mineral phases exist within this particle. Based on the CCSEM/EDX results in Figure 4, it is likely that many other individual particles also contain a mixture of mineral phases. If the origin of the ice nucleating ability above approximately –15 °C for alkali feldspars is the grain boundary between exsolved phases, as posited by Whale et al. (2017), then it seems reasonable that the grain boundary between more distinct mineral phases could fulfill the same role and serve as a high-activity ice-active site. Thus, whether a potassium rich alkali feldspar shares a grain boundary with a sodium rich alkali feldspar, a plagioclase feldspar, or another mineral phase entirely, the grain boundary will be a higher energy site more prone to chemical dissolution. The specific mineral identity of the two phases would likely play a role, as the phase itself and the lattice match between the phases will influence dissolution kinetics at the grain boundary and the chemical sites exposed within newly formed geometric features. As stated earlier, this dissolution is theorized to create the sites of high IN activity in alkali feldspar minerals.[41] This line of reasoning is hypothetical as we cannot directly test this experimentally using these methods, however this hypothesis could help explain the highly active freezing in the warm temperature regime of –8 to –15 °C that we and others observe in some volcanic ash samples.[10,33]

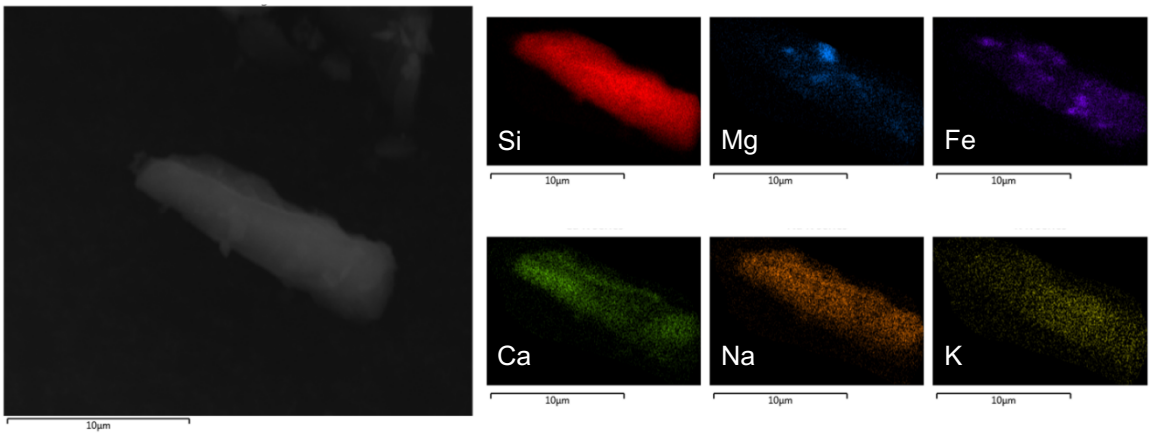


**Figure 5**. SEM image (far left) and EDX elemental maps (K, Mg, Fe, Ca, Na, K) of a single ash particle from Fuego. The particle is from the sieved <37 μm size fraction.

### 3.2 Size-fractionated Fuego Ash and Effects of Particle Mechanical Re-Suspension

A clear trend exists in the XRD composition of the size-separated ash samples, with the amount of Ca-rich and K-rich feldspar decreasing and the amount of Na-rich feldspar and pyroxene increasing as particle size decreases (Table 1). Frozen fraction curves and $n_S$ plots for all four Fuego ash samples are shown in Figure 6. In this figure a trend is also visible where the smaller size-fraction suspensions start and finish freezing at warmer temperatures. The smallest size fraction, PM2.5 and smaller, also possesses higher $n_S$ values than the other size fractions. This suggests that ash freezing ability increases towards smaller particle sizes, although the differences are small – only a couple of degrees Celsius separate the smallest and largest size fractions. Based on our earlier compositional analysis, we conclude that the increase in freezing ability is due to the increasing amount of pyroxene minerals towards smaller size fractions.

It is also apparent that all three size segregated ashes possess higher IN activity than the original <37 μm sieved ash that was not re-suspended, based on the earliest and final droplet freezing temperatures and the $n_S$ values. The BET SSA values in Table 1 suggest that the surface of the ash particles changed somewhat during re-suspension and residence in the dust generator, as the surface area-to-mass ratio of each individual size fraction is greater than the ratio for the <37 μm fraction. This is unsurprising, as within the dust generator an air jet is used to resuspend the particles, causing particles to collide with each other or with the chamber walls and thus increase their surface area through mechanical weathering. Mechanical weathering through milling was previously observed to increase the IN activity of some quartz samples,[47,64] while also leaving other quartz and feldspar samples relatively unaffected.[47] Mechanical weathering can fracture or ablate the particle surface, remove coatings or less reactive areas that have formed on the particle due to natural weathering, and potentially break up particles or particle aggregates. Natural weathering can produce coatings or less reactive mineral surfaces[28,29,68] that may be less ice-active than a pristine mineral surface, and volcanic ashes are uniquely prone to natural chemical weathering caused by reactive species, such as water vapor,

sulfur dioxide, and sulfuric acid that are frequently emitted from volcanoes.[69] Mechanical weathering can also create a particle surface that is more reactive and prone to chemical attack,[20] which is necessary to create the topographical features that Whale et al. (2017) posit as the sites of high IN activity in exsolved alkali feldspars[41] and to create the surface functionalization that Kumar et al. (2018) posit as the origin of IN activity in milled quartz.[64] The exact mechanism by which mechanical ablation increases the IN activity of our samples is unclear at this point. In general the magnitude of these mechanical weathering effects will depend on the sample and may not be large, but their potential impacts on surface and ice nucleation properties should be a consideration when performing laboratory experiments utilizing dry resuspension or milling techniques.

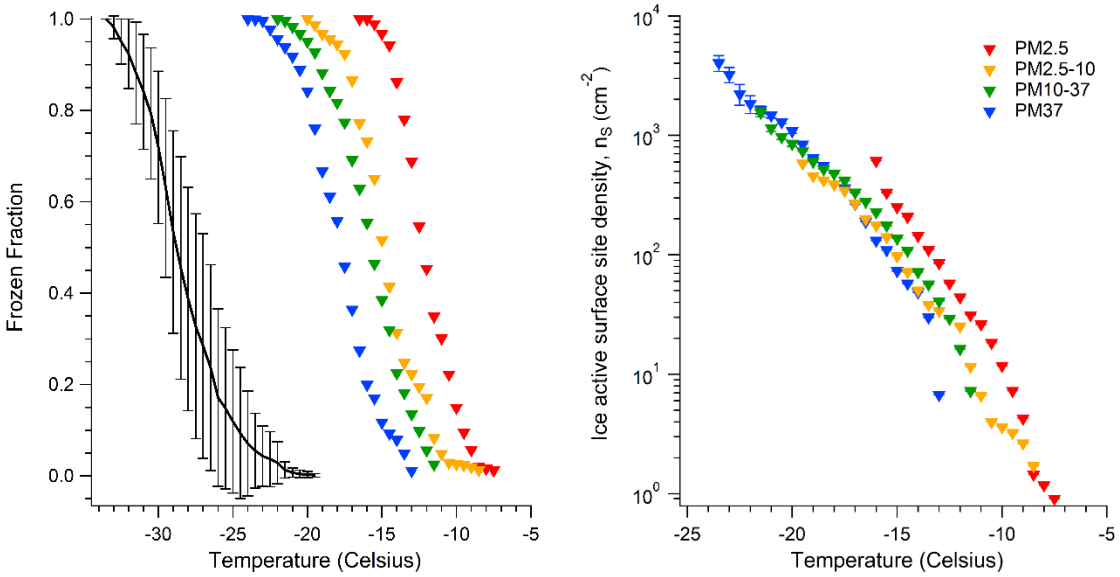


**Figure 6.** Droplet freezing temperature spectra (left), and ice active site density ($n_S$) spectra of the 0.1 wt% size segregated Fuego ash samples and the 0.1 wt% Fugeo <37 μm ash sample. An average purified water background spectrum for the CMU-CS system is shown in black, plotted with error bars representing a single standard deviation. Droplet arrays composed of 0.01 wt% suspensions are omitted to reduce clutter and are instead displayed in Figure S4.

### 3.3 Comparison to Prior Studies of Volcanic Ash Ice Nucleation Properties

A comparison of our $n_S$ spectra with the $n_S$ data for volcanic ash samples compiled by Mangan et al. (2017) is shown in Figure 7.[33] Comparable but weaker IN behavior is observed for SHV ash between this work and that of Mangan et al., however much more active behavior is observed for Fuego and SHV ash compared to that reported by Schill et al. (2015),[32] where the observed immersion-mode freezing temperature of these ashes was low and very close to the background freezing limit of their system.

Compositional differences between ash samples may cause some of the discrepancy between these results. The SHV ash analyzed in the previous work of Mangan et al. (2017) contains more pyroxene than our sample (18.8% vs 12.3%), and so would be expected to possess

slightly higher ice activity based on the activity of the pure pyroxene mineral reported here. No amorphous material was measured in the Mangan et al. sample versus 76% amorphous content in our ash sample. Since volcanic glass is a weaker ice nucleant than the crystalline components of volcanic ash,[34,50] the amorphous material in our sample effectively dilutes the concentration of effective ice nucleants. This reduces the chances of each droplet possessing an effective INP and extends our $n_S$ plots to relatively lower temperatures. Additionally, Mangan et al. describe their results as an upper limit on the ice nucleating ability of SHV ash because they ground their samples and may have exposed fresh, ice-active particle surfaces. To evaluate this possibility, we employed a similar preparation procedure, and analyzed the IN ability of a sample of Fuego ash that was originally >37 μm that we ground and sieved to be <37 μm. The ground and sieved sample started and finished freezing at warmer temperatures than the sieved sample (Figure S5) but the $n_S$ plot did not shift to higher or lower values. Overall, the weaker freezing ability of SHV ash observed in our samples makes sense, as our sample contained less ice-active pyroxene minerals, more amorphous volcanic glass, and was sieved rather than ground.

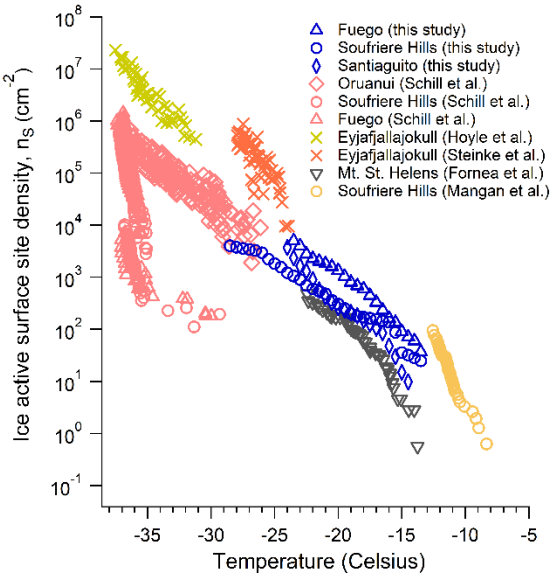


**Figure 7**. Comparison of ice active site density values ($n_S$) obtained in the present work (blue) plotted along with available literature data[32,33,48,49,70]for volcanic ash samples, originally compiled by Mangan et al. (2017).[33] Symbols are consistent between volcanoes and the same color indicates datasets from the same publication.

The origin of the weaker freezing activity for SHV observed by Schill et al. (2015) remains unclear. Compositional differences do exist between ash samples, but the main components of the ashes studied by Schill et al. are still plagioclase feldspars and thus similar to our sample. However, their SHV ashes freeze much colder than would be expected from other work on plagioclase feldspars.[19,37] This suggests that other factors may be affecting the IN ability of these ashes. Mangan et al. (2017) suggested that the difference in activity could be due to the sample preparation method used by Schill et al. where ashes were shaken in water for twelve hours prior

to analysis. Feldspars are well known to weather and partially dissolve in aqueous environments,[68,71] which leaves behind amorphous mineral layers[72–75] and renders the surface less ice-active.[35,76–78] We attempted a similar procedure and suspended a sample of ground Fuego ash in water for 24 hours (with limited stirring and agitation) and observed a deactivation of ash freezing ability (Figure S5), with freezing starting 5 °C colder and finishing 5 °C colder. However, the effect does not appear significant enough to explain the observed discrepancy. It is possible that the intense grinding procedure used by Schill et al., where samples were pulverized for 20 minutes in a dental amalgamator, rendered the ice-active feldspar and pyroxene surfaces in the ash exceptionally vulnerable to chemical attack and amorphization during subsequent suspension in water. The third ash examined by Schill et al. – from Ouranui – contained a significant amount of quartz and nucleated ice well above their background freezing temperature regime. Quartz is posited as the ice-active mineral phase in this ash by both Schill et al. and Mangan et al., which is significant as quartz is more stable than feldspars or pyroxenes and could better survive the grinding and suspension in water processes and retain some IN ability, although continued suspension in water has also been observed to deactivate the IN ability of milled quartz.[64] This would imply that quartz-containing mineral dusts and volcanic ashes may better maintain their IN ability during extended weathering and long-range atmospheric transport, though this remains an ongoing area of research.[64]

## 4 Conclusions

We examined the freezing ability and mineral content of three Central American volcanic ashes. The ashes all contain effective ice nucleants with critical freezing temperatures in the range of –12 to –25 °C and active site densities between $10^1$ and $10^4$ $cm^{-2}$ over this temperature range. This is attributed to the presence of multiple types of ice nucleating mineral phases in each ash sample, distributed heterogeneously amongst the individual particles present. Pyroxene minerals act as the most ice-active phases in these ash samples, followed by Ca-rich plagioclase feldspar, and then volcanic glass. The ice nucleation ability of the volcanic ashes is largely determined by the presence of crystalline mineral phases. The contribution of silica polymorphs, present in the Santiaguito and SHV ashes, remains undetermined. However, the similarities between these two ashes and the ash from Volcán de Fuego suggest that silica polymorphs do not contribute significantly to the overall IN behavior of these ashes. Freezing data from size segregated Fuego ash also supports our conclusion that pyroxene phases are effective ice nucleants. This conclusion is a new finding and merits further investigation. However, the low likelihood of finding pyroxene phases in atmospheric mineral particles outside of volcanic ashes likely limits the overall atmospheric significance of the IN activity of these phases, since pyroxenes are not common to desert and mineral dusts.

Differences between our results and previous literature can be attributed in part to both differences in ash composition and differences in ash sample preparation methods, as our samples were neither ground[33] nor suspended for hours in water prior to freezing experiments.[32]

Our results support in part the idea that volcanic ashes often exhibit similar ranges of freezing temperatures.[10] The most ice-active components of volcanic ashes – alkali feldspars and pyroxenes – nucleate ice at similar temperatures and can dominate the observed freezing behavior of a sample. However, the presence of sufficient amounts of less ice-active material, such as volcanic glass or Ca-feldspars, can effectively dilute the IN ability of more active INP in the sample. The IN ability of one of the ash samples was observed to increase with mechanical weathering following aerosol re-suspension, suggesting either that a natural coating that obscured ice-active sites had been ablated away or that surface roughening or particle breakup created additional or more highly ice-active sites on the ash particles. This is consistent with prior research on which features of feldspar[20,41] and quartz[64] minerals impart high IN activity.[20,41] As noted previously, feldspar, pyroxene, and other phases present in volcanic ash can weather in the presence of reactive species emitted from volcanoes such as water and acidic sulfur gases. The effects of such weathering on the surface and freezing properties of mineral-based INPs remain an important question requiring further research to determine the significance of volcanic ashes as INPs following transport away from the immediate vicinity of the volcano.

## Supporting Information

The supporting material for this publication contains: a description of the dry dust generator and ash size separation protocol; more detailed description of the pyroxene and volcanic ash compositions, accompanied by XRD spectra; and more detailed freezing spectra and active site density plots of the size fractionated Fuego ash and treated Fuego ash samples.

## Acknowledgements

This work was funded by the National Science Foundation (CHE-155494). The authors acknowledge the use of the Materials Characterization Facility at Carnegie Mellon University, supported by the NSF (MCF-677785). D.B. Williams acknowledges funding from the NASA Earth and Space Science Fellowship program, grant number NNX15AQ72H. We thank RJ Lee Group for performing the polarized light microscopy analysis.

## References

(1) Murray, B. J.; O'Sullivan, D.; Atkinson, J. D.; Webb, M. E. Ice Nucleation by Particles Immersed in Supercooled Cloud Droplets. *Chem. Soc. Rev.* **2012**, *41* (19), 6519–6554. https://doi.org/10.1039/c2cs35200a.

(2) Cashman, K.; Rust, A. Volcanic Ash: Generation and Spatial Variations. In *Volcanic Ash*; Mackie, S., Cashman, K., Ricketts, H., Rust, A., Watson, M., Eds.; Elsevier, 2016; pp 5–22. https://doi.org/https://doi.org/10.1016/B978-0-08-100405-0.00002-1.

(3) Lyons, J. J.; Waite, G. P.; Rose, W. I.; Chigna, G. Patterns in Open Vent, Strombolian Behavior at Fuego Volcano, Guatemala, 2005-2007. *Bull. Volcanol.* **2010**, *72* (1), 1–15. https://doi.org/10.1007/s00445-009-0305-7.

(4) Martin, D. P.; Rose, W. I. Behavioral Patterns of Fuego Volcano, Guatemala. *J. Volcanol. Geotherm. Res.* **1981**, *10* (1–3), 67–81. https://doi.org/10.1016/0377-0273(81)90055-X.

(5) Hobbs, P. V; Fullerton, C. M.; Bluhm, G. C. Ice Nucleus Storms in Hawaii. *Nat. Phys. Sci.* **1971**, *230*, 90–91.

(6) Rolf, C.; Krämer, M.; Schiller, C.; Hildebrandt, M.; Riese, M. Lidar Observation and Model Simulation of a Volcanic-Ash-Induced Cirrus Cloud during the Eyjafjallajökull Eruption. *Atmos. Chem. Phys.* **2012**, *12* (21), 10281–10294. https://doi.org/10.5194/acp-12-10281-2012.

(7) Durant, A. J.; Rose, W. I.; Sarna-Wojcicki, A. M.; Carey, S.; Volentik, A. C. M. Hydrometeor-Enhanced Tephra Sedimentation: Constraints from the 18 May 1980 Eruption of Mount St. Helens. *J. Geophys. Res.* **2009**, *114* (B3), B03204. https://doi.org/10.1029/2008JB005756.

(8) van Eaton, A. R.; Muirhead, J. D.; Wilson, C. J. N.; Cimarelli, C. Growth of Volcanic Ash Aggregates in the Presence of Liquid Water and Ice: An Experimental Approach. *Bull. Volcanol.* **2012**, *74* (9), 1963–1984. https://doi.org/10.1007/s00445-012-0634-9.

(9) Van Eaton, A. R.; Mastin, L. G.; Herzog, M.; Schwaiger, H. F.; Schneider, D. J.; Wallace, K. L.; Clarke, A. B. Hail Formation Triggers Rapid Ash Aggregation in Volcanic Plumes. *Nat. Commun.* **2015**, *6*, 1–7. https://doi.org/10.1038/ncomms8860.

(10) Durant, A. J.; Shaw, R. A.; Rose, W. I.; Mi, Y.; Ernst, G. G. J. Ice Nucleation and Overseeding of Ice in Volcanic Clouds. *J. Geophys. Res. Atmos.* **2008**, *113* (9), D09206. https://doi.org/10.1029/2007JD009064.

(11) McNutt, S. R.; Williams, E. R. Volcanic Lightning: Global Observations and Constraints on Source Mechanisms. *Bull. Volcanol.* **2010**, *72* (10), 1153–1167. https://doi.org/10.1007/s00445-010-0393-4.

(12) Engwell, S.; Eychenne, J. Contribution of Fine Ash to the Atmosphere From Plumes Associated With Pyroclastic Density Currents. In *Volcanic Ash*; Mackie, S., Cashman, K., Ricketts, H., Rust, A., Watson, M., Eds.; Elsevier, 2016; pp 67–85. https://doi.org/https://doi.org/10.1016/B978-0-08-100405-0.00007-0.

(13) Seifert, P.; Ansmann, A.; Groß, S.; Freudenthaler, V.; Heinold, B.; Hiebsch, A.; Mattis, I.; Schmidt, J.; Schnell, F.; Tesche, M.; et al. Ice Formation in Ash-Influenced Clouds after the Eruption of the Eyjafjallajkull Volcano in April 2010. *J. Geophys. Res. Atmos.* **2011**, *116* (18), 1–14. https://doi.org/10.1029/2011JD015702.

(14) Pedevilla, P.; Fitzner, M.; Michaelides, A. What Makes a Good Descriptor for Heterogeneous Ice Nucleation on OH-Patterned Surfaces. *Phys. Rev. B* **2017**, *96* (11), 115441. https://doi.org/10.1103/PhysRevB.96.115441.

(15) Freedman, M. A. Potential Sites for Ice Nucleation on Aluminosilicate Clay Minerals and Related Materials. *J. Phys. Chem. Lett.* **2015**, *6* (19), 3850–3858.

https://doi.org/10.1021/acs.jpclett.5b01326.

(16) Kanji, Z. A.; Florea, O.; Abbatt, J. P. D. Ice Formation via Deposition Nucleation on Mineral Dust and Organics: Dependence of Onset Relative Humidity on Total Particulate Surface Area. *Environ. Res. Lett.* **2008**, *3* (2). https://doi.org/10.1088/1748-9326/3/2/025004.

(17) Pedevilla, P.; Cox, S. J.; Slater, B.; Michaelides, A. Can Ice-Like Structures Form on Non-Ice-Like Substrates? The Example of the K-Feldspar Microcline. *J. Phys. Chem. C* **2016**, *120* (12), 6704–6713. https://doi.org/10.1021/acs.jpcc.6b01155.

(18) Sosso, G. C.; Li, T.; Donadio, D.; Tribello, G. A.; Michaelides, A. Microscopic Mechanism and Kinetics of Ice Formation at Complex Interfaces: Zooming in on Kaolinite. *J. Phys. Chem. Lett.* **2016**, *7* (13), 2350–2355. https://doi.org/10.1021/acs.jpclett.6b01013.

(19) Peckhaus, A.; Kiselev, A.; Hiron, T.; Ebert, M.; Leisner, T. A Comparative Study of K-Rich and Na/Ca-Rich Feldspar Ice-Nucleating Particles in a Nanoliter Droplet Freezing Assay. *Atmos. Chem. Phys.* **2016**, *16* (18), 11477–11496. https://doi.org/10.5194/acp-16-11477-2016.

(20) Kiselev, A.; Bachmann, F.; Pedevilla, P.; Cox, S. J.; Michaelides, A.; Gerthsen, D.; Leisner, T. Active Sites in Heterogeneous Ice Nucleation—the Example of K-Rich Feldspars. *Science.* **2017**, *355* (6323), 367–371. https://doi.org/10.1126/science.aai8034.

(21) Abdelmonem, A.; Backus, E. H. G.; Hoffmann, N.; Sánchez, M. A.; Cyran, J. D.; Kiselev, A.; Bonn, M. Surface-Charge-Induced Orientation of Interfacial Water Suppresses Heterogeneous Ice Nucleation on **α**-Alumina (0001). *Atmos. Chem. Phys.* **2017**, *17* (12), 7827–7837. https://doi.org/10.5194/acp-17-7827-2017.

(22) Marcolli, C.; Nagare, B.; Welti, A.; Lohmann, U. Ice Nucleation Efficiency of AgI: Review and New Insights. *Atmos. Chem. Phys.* **2016**, *16* (14), 8915–8937. https://doi.org/10.5194/acp-16-8915-2016.

(23) Kanji, Z. A.; Ladino, L. A.; Wex, H.; Boose, Y.; Burkert-Kohn, M.; Cziczo, D. J.; Krämer, M. Overview of Ice Nucleating Particles. *Meteorol. Monogr.* **2017**, *58*, 1.1-1.33. https://doi.org/10.1175/AMSMONOGRAPHS-D-16-0006.1.

(24) Glatz, B.; Sarupria, S. Heterogeneous Ice Nucleation: Interplay of Surface Properties and Their Impact on Water Orientations. *Langmuir* **2018**, *34* (3), 1190–1198. https://doi.org/10.1021/acs.langmuir.7b02859.

(25) Horwell, C. J.; Sparks, R. S. J.; Brewer, T. S.; Llewellin, E. W.; Williamson, B. J. Characterization of Respirable Volcanic Ash from the Soufrière Hills Volcano, Montserrat, with Implications for Human Health Hazards. *Bull. Volcanol.* **2003**, *65* (5), 346–362. https://doi.org/10.1007/s00445-002-0266-6.

(26) Nakagawa, M.; Ohba, T. Minerals in Volcanic Ash 1: Primary Minerals and Volcanic Glass. *Glob. Environ. Res.* **2002**, 41–51.

(27) Eggleton, R. A. Weathering of Basalt: Changes in Rock Chemistry and Mineralogy. *Clays Clay Miner.* **1987**, *35* (3), 161–169. https://doi.org/10.1346/CCMN.1987.0350301.

(28) Parkin, G. W.; Gardner, W. H.; Auerswald, K.; Bouma, J.; Chesworth, W. Weathering Systems in Soil Science. In *Encyclopedia of Soil Science*; Chesworth, W., Ed.; Encyclopedia of Earth Sciences Series; Springer Netherlands: Dordrecht, 2008; pp 825–830. https://doi.org/10.1007/978-1-4020-3995-9_633.

(29) Blum, A. E. Feldspars in Weathering. In *Feldspars and their Reactions*; Parsons, I., Ed.; Springer Netherlands: Dordrecht, 1994; pp 595–630. https://doi.org/10.1007/978-94-011-1106-5_15.

(30) Perlwitz, J. P.; Pérez García-Pando, C.; Miller, R. L. Predicting the Mineral Composition of Dust Aerosols – Part 1: Representing Key Processes. *Atmos. Chem. Phys.* **2015**, *15* (20), 11593–11627. https://doi.org/10.5194/acp-15-11593-2015.

(31) Perlwitz, J. P.; Pérez García-Pando, C.; Miller, R. L. Predicting the Mineral Composition of Dust Aerosols - Part 2: Model Evaluation and Identification of Key Processes with Observations. *Atmos. Chem. Phys.* **2015**, *15* (20), 11629–11652. https://doi.org/10.5194/acp-15-11629-2015.

(32) Schill, G. P.; Genareau, K.; Tolbert, M. A. Deposition and Immersion-Mode Nucleation of Ice by Three Distinct Samples of Volcanic Ash. *Atmos. Chem. Phys.* **2015**, *15* (13), 7523–7536. https://doi.org/10.5194/acp-15-7523-2015.

(33) Mangan, T. P.; Atkinson, J. D.; Neuberg, J. W.; O'Sullivan, D.; Wilson, T. W.; Whale, T. F.; Neve, L.; Umo, N. S.; Malkin, T. L.; Murray, B. J. Heterogeneous Ice Nucleation by Soufriere Hills Volcanic Ash Immersed in Water Droplets. *PLoS One* **2017**, *12* (1), 1–11. https://doi.org/10.1371/journal.pone.0169720.

(34) Kulkarni, G.; Nandasiri, M.; Zelenyuk, A.; Beranek, J.; Madaan, N.; Devaraj, A.; Shutthanandan, V.; Thevuthasan, S.; Varga, T. Effects of Crystallographic Properties on the Ice Nucleation Properties of Volcanic Ash Particles. *Geophys. Res. Lett.* **2015**, *42* (8), 3048–3055. https://doi.org/10.1002/2015GL063270.

(35) Atkinson, J. D.; Murray, B. J.; Woodhouse, M. T.; Whale, T. F.; Baustian, K. J.; Carslaw, K. S.; Dobbie, S.; O'Sullivan, D.; Malkin, T. L. The Importance of Feldspar for Ice Nucleation by Mineral Dust in Mixed-Phase Clouds. *Nature* **2013**, *498* (7454), 355–358. https://doi.org/10.1038/nature12278.

(36) Vergara-Temprado, J.; Murray, B. J.; Wilson, T. W.; O'Sullivan, D.; Browse, J.; Pringle, K. J.; Ardon-Dryer, K.; Bertram, A. K.; Burrows, S. M.; Ceburnis, D.; et al. Contribution of Feldspar and Marine Organic Aerosols to Global Ice Nucleating Particle Concentrations. *Atmos. Chem. Phys.* **2017**, *17* (5), 3637–3658. https://doi.org/10.5194/acp-17-3637-2017.

(37) Harrison, A. D.; Whale, T. F.; Carpenter, M. A.; Holden, M. A.; Neve, L.;

O'Sullivan, D.; Vergara Temprado, J.; Murray, B. J. Not All Feldspars Are Equal: A Survey of Ice Nucleating Properties across the Feldspar Group of Minerals. *Atmos. Chem. Phys.* **2016**, *16* (17), 10927–10940. https://doi.org/10.5194/acp-16-10927-2016.

(38) Yakobi-Hancock, J. D.; Ladino, L. a.; Abbatt, J. P. D. Feldspar Minerals as Efficient Deposition Ice Nuclei. *Atmos. Chem. Phys.* **2013**, *13* (22), 11175–11185. https://doi.org/10.5194/acp-13-11175-2013.

(39) Boose, Y.; Sierau, B.; García, M. I.; Rodríguez, S.; Alastuey, A.; Linke, C.; Schnaiter, M.; Kupiszewski, P.; Kanji, Z. A.; Lohmann, U. Ice Nucleating Particles in the Saharan Air Layer. *Atmos. Chem. Phys.* **2016**, *16* (14), 9067–9087. https://doi.org/10.5194/acp-16-9067-2016.

(40) Kaufmann, L.; Marcolli, C.; Luo, B.; Peter, T. Refreeze Experiments with Water Droplets Containing Different Types of Ice Nuclei Interpreted by Classical Nucleation Theory. *Atmos. Chem. Phys.* **2017**, *17* (5), 3525–3552. https://doi.org/10.5194/acp-17-3525-2017.

(41) Whale, T. F.; Holden, M. A.; Kulak, A. N.; Kim, Y.-Y.; Meldrum, F. C.; Christenson, H. K.; Murray, B. J. The Role of Phase Separation and Related Topography in the Exceptional Ice-Nucleating Ability of Alkali Feldspars. *Phys. Chem. Chem. Phys.* **2017**, *19* (46), 31186–31193. https://doi.org/10.1039/C7CP04898J.

(42) Bi, Y.; Cao, B.; Li, T. Enhanced Heterogeneous Ice Nucleation by Special Surface Geometry. *Nat. Commun.* **2017**, *8*. https://doi.org/10.1038/ncomms15372.

(43) Putnis, A. Transformation Processes in Minerals I: Exsolution. In *An Introduction to Mineral Sciences*; Putnis, A., Ed.; Cambridge University Press: Cambridge, 1992; pp 333–386. https://doi.org/DOI: 10.1017/CBO9781139170383.013.

(44) Poldervaart, A.; Hess, H. H. Pyroxenes in the Crystallization of Basaltic Magma. *J. Geol.* **1951**, *59* (5), 472–489.

(45) Maters, E. C.; Dingwell, D. B.; Cimarelli, C.; Müller, D.; Whale, T. F.; Murray, B. J. The Importance of Crystalline Phases in Ice Nucleation by Volcanic Ash. *Atmos. Chem. Phys. Discuss.* **2019**, No. January, 1–19. https://doi.org/10.5194/acp-2018-1326.

(46) Isono, K.; Ikebe, Y. On the Ice-Nucleating Ability of Rock-Forming Minerals and Soil Particles. *J. Meteorol. Soc. Japan* **1960**, *38* (5), 213–320.

(47) Zolles, T.; Burkart, J.; Häusler, T.; Pummer, B.; Hitzenberger, R.; Grothe, H. Identification of Ice Nucleation Active Sites on Feldspar Dust Particles. *J. Phys. Chem. A* **2015**, *119* (11), 2692–2700. https://doi.org/10.1021/jp509839x.

(48) Steinke, I.; Möhler, O.; Kiselev, A.; Niemand, M.; Saathoff, H.; Schnaiter, M.; Skrotzki, J.; Hoose, C.; Leisner, T. Ice Nucleation Properties of Fine Ash Particles from the Eyjafjallajökull Eruption in April 2010. *Atmos. Chem. Phys.* **2011**, *11* (24), 12945–12958. https://doi.org/10.5194/acp-11-12945-2011.

(49) Hoyle, C. R.; Pinti, V.; Welti, A.; Zobrist, B.; Marcolli, C.; Luo, B.; ?oskuldsson, Á.; Mattsson, H. B.; Stetzer, O.; Thorsteinsson, T.; et al. Ice Nucleation Properties of Volcanic Ash from Eyjafjallajökull. *Atmos. Chem. Phys.* **2011**, *11* (18), 9911–9926. https://doi.org/10.5194/acp-11-9911-2011.

(50) Gibbs, A.; Charman, M.; Schwarzacher, W.; Rust, A. C. Immersion Freezing of Supercooled Water Drops Containing Glassy Volcanic Ash Particles. *GeoResJ* **2015**, *7*, 66–69. https://doi.org/10.1016/j.grj.2015.06.002.

(51) Williams, D. B. An Analysis of Proximal Volcanic Ash Emissions, University of Pittsburgh, 2018.

(52) Sullivan, R. C.; Guazzotti, S. a.; Sodeman, D. a.; Prather, K. a. Direct Observations of the Atmospheric Processing of Asian Mineral Dust. *Atmos. Chem. Phys.* **2007**, *7* (5), 1213–1236. https://doi.org/10.5194/acp-7-1213-2007.

(53) Polen, M.; Lawlis, E.; Sullivan, R. C. The Unstable Ice Nucleation Properties of Snomax® Bacterial Particles. *J. Geophys. Res. Atmos.* **2016**, *121* (19), 11,666-11,678. https://doi.org/10.1002/2016JD025251.

(54) Polen, M.; Brubaker, T.; Somers, J.; Sullivan, R. C. Cleaning up Our Water: Reducing Interferences from Nonhomogeneous Freezing of "Pure" Water in Droplet Freezing Assays of Ice-Nucleating Particles. *Atmos. Meas. Tech.* **2018**, *11* (9), 5315–5334. https://doi.org/10.5194/amt-11-5315-2018.

(55) Beydoun, H.; Polen, M.; Sullivan, R. C. Effect of Particle Surface Area on Ice Active Site Densities Retrieved from Droplet Freezing Spectra. *Atmos. Chem. Phys.* **2016**, *16* (20), 13359–13378. https://doi.org/10.5194/acp-16-13359-2016.

(56) Vali, G. Quantitative Evaluation of Experimental Results an the Heterogeneous Freezing Nucleation of Supercooled Liquids. *Journal of the Atmospheric Sciences*. 1971, pp 402–409. https://doi.org/10.1175/1520-0469(1971)028<0402:QEOERA>2.0.CO;2.

(57) Hoose, C.; Möhler, O. Heterogeneous Ice Nucleation on Atmospheric Aerosols: A Review of Results from Laboratory Experiments. *Atmos. Chem. Phys.* **2012**, *12* (20), 9817–9854. https://doi.org/10.5194/acp-12-9817-2012.

(58) O'Sullivan, D.; Murray, B. J.; Ross, J. F.; Whale, T. F.; Price, H. C.; Atkinson, J. D.; Umo, N. S.; Webb, M. E. The Relevance of Nanoscale Biological Fragments for Ice Nucleation in Clouds. *Sci. Rep.* **2015**, *5* (1), 8082. https://doi.org/10.1038/srep08082.

(59) Emersic, C.; Connolly, P. J.; Boult, S.; Campana, M.; Li, Z. Investigating the Discrepancy between Wet-Suspension- and Dry-Dispersion-Derived Ice Nucleation Efficiency of Mineral Particles. *Atmos. Chem. Phys.* **2015**, *15* (19), 11311–11326. https://doi.org/10.5194/acp-15-11311-2015.

(60) Wex, H.; Augustin-Bauditz, S.; Boose, Y.; Budke, C.; Curtius, J.; Diehl, K.; Dreyer, A.; Frank, F.; Hartmann, S.; Hiranuma, N.; et al. Intercomparing Different Devices for the

Investigation of Ice Nucleating Particles Using Snomax® as Test Substance. *Atmos. Chem. Phys.* **2015**, *15* (3), 1463–1485. https://doi.org/10.5194/acp-15-1463-2015.

(61) Hiranuma, N.; Augustin-Bauditz, S.; Bingemer, H.; Budke, C.; Curtius, J.; Danielczok, A.; Diehl, K.; Dreischmeier, K.; Ebert, M.; Frank, F.; et al. A Comprehensive Laboratory Study on the Immersion Freezing Behavior of Illite NX Particles: A Comparison of 17 Ice Nucleation Measurement Techniques. *Atmos. Chem. Phys.* **2015**, *15* (5), 2489–2518. https://doi.org/10.5194/acp-15-2489-2015.

(62) Peckhaus, A.; Kiselev, A.; Hiron, T.; Ebert, M.; Leisner, T. A Comparative Study of K-Rich and Na/Ca-Rich Feldspar Ice-Nucleating Particles in a Nanoliter Droplet Freezing Assay. *Atmos. Chem. Phys.* **2016**, *16* (18), 11477–11496. https://doi.org/10.5194/acp-16-11477-2016.

(63) Deer, W. A.; Howie, R. A.; Wise, W. S.; Zussman, J. *Rock-Forming Minerals: Silica Minerals, Volume 4B*, 2nd ed.; The Geological Society of London, 2004.

(64) Kumar, A.; Marcolli, C.; Peter, T. Ice Nucleation Activity of Silicates and Aluminosilicates in Pure Water and Aqueous Solutions. Part 2 - Quartz and Amorphous Silica. *Atmos. Chem. Phys. Discuss.* **2018**, 1–35. https://doi.org/10.5194/acp-2018-1020.

(65) Whale, T. F.; Holden, M. A.; Wilson, T. W.; O'Sullivan, D.; Murray, B. J. The Enhancement and Suppression of Immersion Mode Heterogeneous Ice-Nucleation by Solutes. *Chem. Sci.* **2018**, *9*, 4142–4151. https://doi.org/10.1039/c7sc05421a.

(66) Robinson, P.; Ross, M.; Nord, G. L.; Smyth, J. R.; Jaffe, H. W. Exsolution Lamellae in Augite and Pigeonite: Fossil Indicators of Iattice Parameters at High Temperature and Pressure. *Am. Mineral.* **1977**, *62*, 857–873.

(67) Yuan, H.; Rahn, K. A.; Zhuang, G. Graphical Techniques for Interpreting the Composition of Individual Aerosol Particles. *Atmos. Environ.* **2004**, *38* (39), 6845–6854. https://doi.org/https://doi.org/10.1016/j.atmosenv.2004.09.010.

(68) Zhu, C. In Situ Feldspar Dissolution Rates in an Aquifer. *Geochim. Cosmochim. Acta* **2005**, *69* (6), 1435–1449. https://doi.org/10.1016/j.gca.2004.09.005.

(69) Textor, C.; Graf, H.-F.; Timmreck, C.; Robock, A. Emissions from Volcanoes. In *Emissions of atmospheric trace compounds*; Springer, 2004; pp 269–303. https://doi.org/10.1007/978-1-4020-2167-1_7.

(70) Fornea, A. P.; Brooks, S. D.; Dooley, J. B.; Saha, A. Heterogeneous Freezing of Ice on Atmospheric Aerosols Containing Ash, Soot, and Soil. *J. Geophys. Res. Atmos.* **2009**, *114* (13), 1–12. https://doi.org/10.1029/2009JD011958.

(71) Helgeson, H. C.; Murphy, W. M.; Aagaard, P. Thermodynamic and Kinetic Constraints on Reaction Rates among Minerals and Aqueous Solutions. II. Rate Constants, Effective Surface Area, and the Hydrolysis of Feldspar. *Geochim. Cosmochim. Acta* **1984**, *48* (12), 2405–2432. https://doi.org/10.1016/0016-7037(84)90294-1.

(72) Yang, Y.; Min, Y.; Lococo, J.; Jun, Y.-S. Effects of Al/Si Ordering on Feldspar Dissolution: Part I. Crystallographic Control on the Stoichiometry of Dissolution Reaction. *Geochim. Cosmochim. Acta* **2014**, *126*, 574–594. https://doi.org/10.1016/j.gca.2013.10.047.

(73) Marshall, C. E. Reactions of Feldspars and Micas with Aqueous Solutions. *Econ. Geol.* **1962**, *57* (8), 1219–1227. https://doi.org/10.2113/gsecongeo.57.8.1219.

(74) Stillings, L. L.; Brantley, S. L. Feldspar Dissolution at 25°C and PH 3: Reaction Stoichiometry and the Effect of Cations. *Geochim. Cosmochim. Acta* **1995**, *59* (8), 1483–1496. https://doi.org/10.1016/0016-7037(95)00057-7.

(75) Chemtob, S. M.; Rossman, G. R. Timescales and Mechanisms of Formation of Amorphous Silica Coatings on Fresh Basalts at Kīlauea Volcano, Hawai'i. *J. Volcanol. Geotherm. Res.* **2014**, *286*, 41–54. https://doi.org/10.1016/j.jvolgeores.2014.08.029.

(76) Augustin-Bauditz, S.; Wex, H.; Kanter, S.; Ebert, M.; Niedermeier, D.; Stolz, F.; Prager, A.; Stratmann, F. The Immersion Mode Ice Nucleation Behavior of Mineral Dusts: A Comparison of Different Pure and Surface Modified Dusts. *Geophys. Res. Lett.* **2014**, *41* (20), 7375–7382. https://doi.org/10.1002/2014GL061317.

(77) Kumar, A.; Marcolli, C.; Luo, B.; Peter, T. Ice Nucleation Activity of Silicates and Aluminosilicates in Pure Water and Aqueous Solutions – Part 1: The K-Feldspar Microcline. *Atmos. Chem. Phys.* **2018**, *18* (10), 7057–7079. https://doi.org/10.5194/acp-18-7057-2018.

(78) Kumar, A.; Marcolli, C.; Peter, T. Ice Nucleation Activity of Silicates and Aluminosilicates in Pure Water and Aqueous Solutions. Part 3 – Aluminosilicates. *Atmos. Chem. Phys. Discuss.* **2018**, *18* (10), 1–36. https://doi.org/10.5194/acp-2018-1021.

## TOC Art